Improving Li-ion interfacial transport in hybrid solid electrolytes

Liu, Ming; Zhang, Shengnan; van Eck, Ernst R.H.; Wang, Chao; Ganapathy, Swapna; Wagemaker, Marnix

DOI
10.1038/s41565-022-01162-9

Publication date
2022

Document Version
Accepted author manuscript

Published in
Nature Nanotechnology

Citation (APA)
Liu, M., Zhang, S., van Eck, E. R. H., Wang, C., Ganapathy, S., & Wagemaker, M. (2022). Improving Li-ion interfacial transport in hybrid solid electrolytes. *Nature Nanotechnology*, *17*(9), 959-967. https://doi.org/10.1038/s41565-022-01162-9

Improving Li-ion Interfacial Transport in Hybrid Solid Electrolytes

Ming Liu[a], Shengnan Zhang[a], Ernst R. H. van Eck[b], Chao Wang[a], Swapna Ganapathy[a*], Marnix Wagemaker[a*]

[a] Section Storage of Electrochemical Energy, Radiation Science and Technology, Faculty of Applied Sciences, Delft University of Technology, Mekelweg 15, 2629 JB, Delft, The Netherlands.

E-mail: s.ganapathy@tudelft.nl and m.wagemaker@tudelft.nl

[b] Institute for Molecules and Materials, Radboud University, Heyendaalseweg 135, 6525 AJ, Nijmegen, The Netherlands.

Abstract

The development of commercial solid-state batteries has to date been hindered by the individual limitations of inorganic and organic solid electrolytes, motivating hybrid concepts. However, the room-temperature conductivity of hybrid solid electrolytes is still insufficient to support the required battery performance. A key challenge is to assess the Li-ion transport over the inorganic and organic interfaces and relate this to surface chemistry. Here we study the interphase structure and the Li-ion transport across the interface of hybrid solid electrolytes using solid-state nuclear magnetic resonance spectroscopy. In a hybrid solid polyethylene oxide polymer – inorganic electrolyte, we introduce two representative types of ionic liquids having a different miscibility with the polymer. The poorly miscible ionic liquid wets the polymer-inorganic interface and increases the local polarizability, thereby lowering the diffusional barrier, resulting in an overall room temperature conductivity of 2.47×10^{-4} S/cm. A critical current density of 0.25 mA/cm^2 versus a Li-metal anode shows improved stability, allowing cycling of a $LiFePO_4$ – Li-metal solid-state cell at room temperature with a Coulombic efficiency of 99.9%. Tailoring the local interface environment between the inorganic and organic solid electrolyte components in hybrid solid electrolytes appears a viable route towards designing highly conducting hybrid solid electrolytes.

Solid-state batteries are recognized as a key candidate for next generation batteries because of their potential to improve both energy density and safety.[1,2] However, the progress in their development is hindered by the many criteria that solid electrolytes must satisfy to become commercially viable. These include high ionic conductivity, flexibility, (electro)chemical stability, compatibility with electrode materials and process-ability, conditions which are often hard to fulfill with an individual organic or inorganic solid electrolyte material.[3-7] This has led to the investigation of hybrid electrolyte concepts, that typically combine an organic and an inorganic phase.[8-11] An intensively investigated hybrid solid electrolyte (HSE) comprises of inorganic filler particles embedded in a conductive organic polymer matrix. The use of polyethylene oxide (PEO) as the organic polymer component together with a Li containing salt is attractive because of its relative stability towards lithium metal, excellent contact/adhesion with electrodes, superior mechanical properties, and good flexibility allowing facile production as thin films on a large scale.[12-17] Properties such as particle size, relative amount and morphology of the inorganic component influence the conductivity of the HSE. Typically inorganic fillers are added to lower the glass transition temperature (T_g) of PEO, thereby enhancing the polymer chain segmental mobility, resulting in higher ionic conductivity.[13,18-20]

More recently, HSEs with inorganic ionic conductors as additives have been investigated aiming to provide highly conductive pathways for Li-ion transport to improve the overall conductivity of the HSE.[18,20-24] However, despite the high ionic conductivity of these inorganic fillers (e.g. > 1 mS/cm), their room temperature Li-ion conductivity remains far from what is demanded for all-solid-state-batteries (~1 mS/cm). This raises questions about the Li-ion transport pathway through the heterogeneous HSE, and especially on the role of the interface between the organic and inorganic components. However, it is challenging to monitor the Li-ion transport in HSEs at the sub-nano scale of interfaces. Several approaches have been reported which explore the correlation between interface environment and Li-ion movement in HSEs.[4,18,25-28] Three-dimensional (3D) structural reconstruction of HSEs obtained from synchrotron experiments and physics-based modeling indicate that the inorganic particles are highly aggregated in the electrolyte, which would affect the internal Li-ion transport between different phases.[4,25] Four-point electrochemical impedance measurements and surface-sensitive X-ray photoelectron spectroscopy revealed decomposition reactions between the organic and inorganic phases, which may significantly affect the

Li-ion transport.[26,27] Recently, combining selective isotope labeling with high-resolution solid-state nuclear magnetic resonance (NMR), Li-ion diffusion pathways were tracked within a $Li_7La_3Zr_2O_{12}$ (LLZO)-PEO HSE.[18,28] While these studies provide insight into Li-ion transport in HSEs, it is also evident that it remains a challenge to directly access the interfacial structure, correlate this to the Li-ion transport across the interface and use this to develop strategies to improve the conductivity of HSEs.[10]

To gain deeper insight into the Li-ion transport in HSEs in conjunction with the inorganic-organic interphase structure, we employed an experimental approach using electrochemical impedance spectroscopy (EIS) and multinuclear solid-state NMR. This allows us to measure the bulk conductivity as well as directly access the interphase structure and interfacial Li-ion diffusion in an HSE comprising of an LiTFSI (lithium-bis (trifluoromethane-sulfonyl)imide)-PEO organic and argyrodite Li_6PS_5Cl inorganic component. We find that the ionic conductivity of the HSE is impeded by the chemical structure of the decomposition layer between the organic and inorganic phases. To overcome this the interface is 'activated' by adding an ionic liquid that settles at the organic-inorganic interface of the HSE, because it is poorly miscible with PEO. This enables Li-ion diffusion over the interface as visualized by two-dimensional (2D) ^{7}Li exchange NMR which increases the overall ionic conductivity of the HSE. Solid-state NMR is demonstrated to be a powerful method for resolving the sub-nano domains of the interface, impossible by other traditional characterization techniques. In this manner the bottleneck for Li-ion transport in HSEs is revealed, and new design strategies are proposed towards future solid electrolytes.

Interphase structure and Li-ion diffusion in the hybrid LiTFSI-PEO-Li_6PS_5Cl solid electrolyte

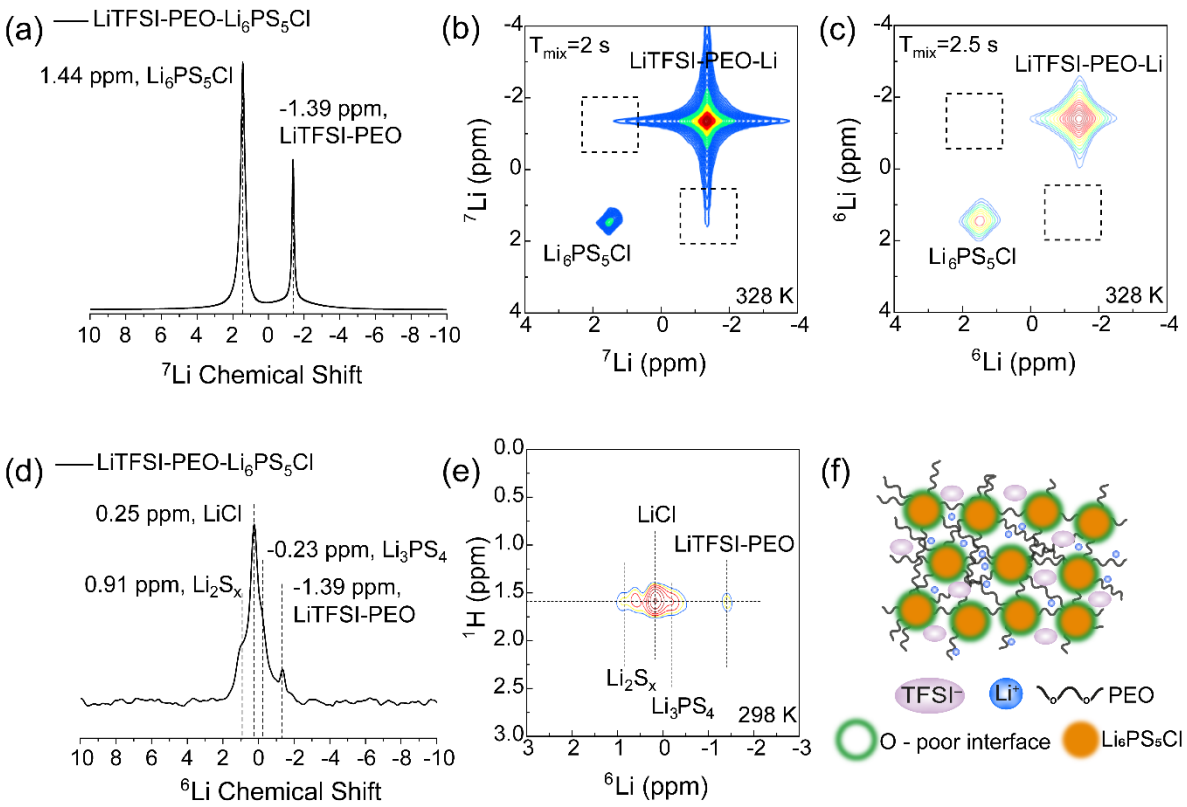

Figure 1 Li-ion interface diffusion between LiTFSI-PEO and Li_6PS_5Cl (a-c) One-dimensional (1D) (a) ^7Li magic angle spinning (MAS) spectrum and two-dimensional (2D) (b) ^7Li–^7Li and (c) ^6Li–^6Li exchange spectra (2D-EXSY) corresponding to the LiTFSI-PEO-Li_6PS_5Cl HSE with mixing times of 2 and 2.5 s at 328 K, where no obvious off-diagonal cross-peak intensity is observed, indicating that the exchange flux of Li-ions over the solid–solid LiTFSI-PEO-Li_6PS_5Cl interface is very small. (d) 1D ^1H-^6Li CPMAS spectrum with a contact time of 6 ms (200 µs – 6 ms can be found in **Figure S2**), measured at a spinning speed of 5 kHz. 1024 scans were acquired with a recycle delay of 20 s. (e) A 2D ^1H-^6Li heteronuclear correlation (HETCOR) spectrum measured with a CP contact time of 0.2 ms. (f) Schematic figure of Li-ion diffusion pathway in the HSE.

With the aim of improving the overall Li-ion conductivity of a LiTFSI-PEO polymer electrolyte, highly conductive micron sized argyrodite Li_6PS_5Cl (5.6 mS/cm) is mixed in the LiTFSI-PEO with a weight fraction of 10 % (SEM images in Supplementary **Figure S1**). For Li_6PS_5Cl to contribute to the bulk conductivity of this HSE, facile Li-ion diffusion over the interfaces between the LiTFSI-PEO phase and the Li_6PS_5Cl particles is a prerequisite. This is because a 10% weight fraction (8% volume fraction) will not result in percolating transport pathways through the Li_6PS_5Cl phase. Li_6PS_5Cl was selected as the inorganic filler to facilitate interfacial transport, as it possesses both

high ionic conductivity and high ductility, the latter enabling the formation of softer interfaces that facilitate interfacial Li-ion diffusion.[29] To study the Li-ion diffusion across the LiTFSI-PEO–Li_6PS_5Cl interface and to resolve the interphase structure between the organic and inorganic phases, magic angle spinning (MAS) ^{6,7}Li solid-state NMR is employed. This allows us to discriminate between Li-ions in different chemical environments, in this case in the PEO and Li_6PS_5Cl phases.[18,29] As seen in **Figure 1a**, the LiTFSI-PEO and Li_6PS_5Cl show two clear resonances with ^{7}Li chemical shifts of -1.39 and 1.44 ppm, respectively. Based on the difference in ^{6,7}Li chemical shift of the LiTFSI-PEO and Li_6PS_5Cl phases, 2D exchange spectroscopy (2D-EXSY) experiments provide selective and non-invasive quantification of the spontaneous Li-ion diffusion over the solid-solid interface between these phases.[29,30] Li-ion exchange between these two chemical environments would result in off-diagonal cross-peaks at the positions indicated with dotted boxes in **Figure 1b and c**. Increasing the mixing time, T_{mix}, therefore providing more time for the Li-ions to diffuse from one phase to the other, as well as increasing the temperature, is expected to increase the Li-ion exchange flux, and thus the intensity of the off-diagonal cross-peaks.[29] In this case the absence of cross-peaks, even for the maximum T_{mix} and temperature (T_{mix} = 2 s and 2.5 s, 328 K) that can be achieved, indicates that the Li-ion exchange (flux) between LiTFSI-PEO and Li_6PS_5Cl phases does not occur at the timescale of T_{mix}, indicating very slow Li-ion diffusion across the interfaces within this HSE.

To discern the origin of the poor Li-ion diffusion across these interfaces, 1D ^{6}Li cross-polarization MAS (CPMAS) and 2D ^{1}H-^{6}Li heteronuclear correlation (HETCOR) experiments were carried out (**Figure 1d, e**) allowing us to resolve the interface composition and structure. In these experiments, transfer of polarization occurs from protons (^{1}H), in this case abundantly present in the polymer, to any ^{6}Li environment in its near vicinity (few bonds range). This takes place during a varying time interval (contact time), typically in the range of 200 µs – 6 ms (Supplementary **Figure S2**). With direct ^{6,7}Li excitation, only two peaks are resolved as shown in **Figure 1a** for ^{7}Li (**Figure S3** for ^{6}Li). However, in the ^{6}Li CPMAS spectrum several additional resonances between 1 ppm and -1.5 ppm (**Figure 1d**) are resolved. The additional peaks are assigned to Li-containing polysulfides and phosphorus sulfide species,[31,32] based on previous literature.[26,27] This indicates that inorganic decomposition products accumulate at the interface that could inhibit interfacial Li-ion transport. The 2D ^{1}H-^{6}Li

experiment at a short contact time shows correlations between ^{1}H and ^{6}Li species either directly bonded to, or in very close proximity with, each other. At a short contact time of 0.2 ms (**Figure 1e**, in Supplementary **Figure S2** peaks are also visible at 0.2 ms) the different Li species observed are in contact with a single ^{1}H environment at a chemical shift of ~1.6 ppm, which can be assigned to the alkyl $–OCH_2-$ group. This has been identified as the main decomposition product of PEO chains when in contact with Li_6PS_5Cl from XPS studies.[26,27,33] This indicates that there are interfacial reactions between Li_6PS_5Cl and PEO, resulting in an inert environment deficient in ethereal oxygen, that is known to mediate the Li-ion diffusion in PEO (**Figure 1f**). This poorly Li-ion conducting interface environment is held responsible for the absence of Li-ion exchange (**Figure 1b-c**), indicating sluggish Li-ion diffusion between the two electrolyte phases. These findings can potentially explain the difficulties in activating inorganic particles in HSEs,[18] indicating that the interface needs to be improved to enhance the interfacial Li-ion diffusion.

Addition of ionic liquids to enhance the conductivity of the PEO-Li_6PS_5Cl hybrid solid electrolyte

Based on the above findings, it is clear that an inert interface is formed between LiTFSI-PEO and Li_6PS_5Cl which impedes charge transport in the HSE. Traditionally, ionic liquids (ILs) have been used to enhance the segmental motion of PEO chains to increase the Li-ion mobility.[9,34] These ILs do not form strong ionic bonds between their cation and anion moieties and hence possess low solvation energy and remain in a dissociated state. It has been shown in previous studies that imidazole-based ILs are effective in improving the conductivity of PEO, because of their low viscosity and high miscibility in PEO.[34]

To determine whether an IL, added to the HSE has impact on the conductivity and interfacial charge diffusivity between the organic and inorganic phases, two ILs that differ significantly in their viscosity and miscibility with PEO were selected. The first is an imidazole-based IL 1-Ethyl-3-methylimidazolium bis(trifluoromethylsulfonyl)imide (denoted as EMIM-TFSI) (**Figure 2a**) and the second is a piperidinium-based IL 1-Methyl-1-propylpiperidinium bis(trifluoromethylsulfonyl)imide (denoted as PP13-TFSI) (**Figure 2b**). These ILs each have a different miscibility in PEO[35] where the hypothesis is that the poorly miscible PP13-TFSI will be preferably located at the interface with the inorganic Li_6PS_5Cl phase,

aiming to improve the Li-ion diffusion across the interface. In contrast, the highly miscible EMIM-TFSI is anticipated to be distributed homogenously in the HSE and not specifically influence Li-ion transport across the organic-inorganic interface. To test this, a fixed amount of EMIM-TFSI and PP13-TFSI (0.25:1 molar ratio IL:LiTFSI) were added to the LiTFSI-PEO-Li_6PS_5Cl mixture. The HSEs subsequently formed are henceforth referred to as HSE-EMIM and HSE-PP13 respectively.

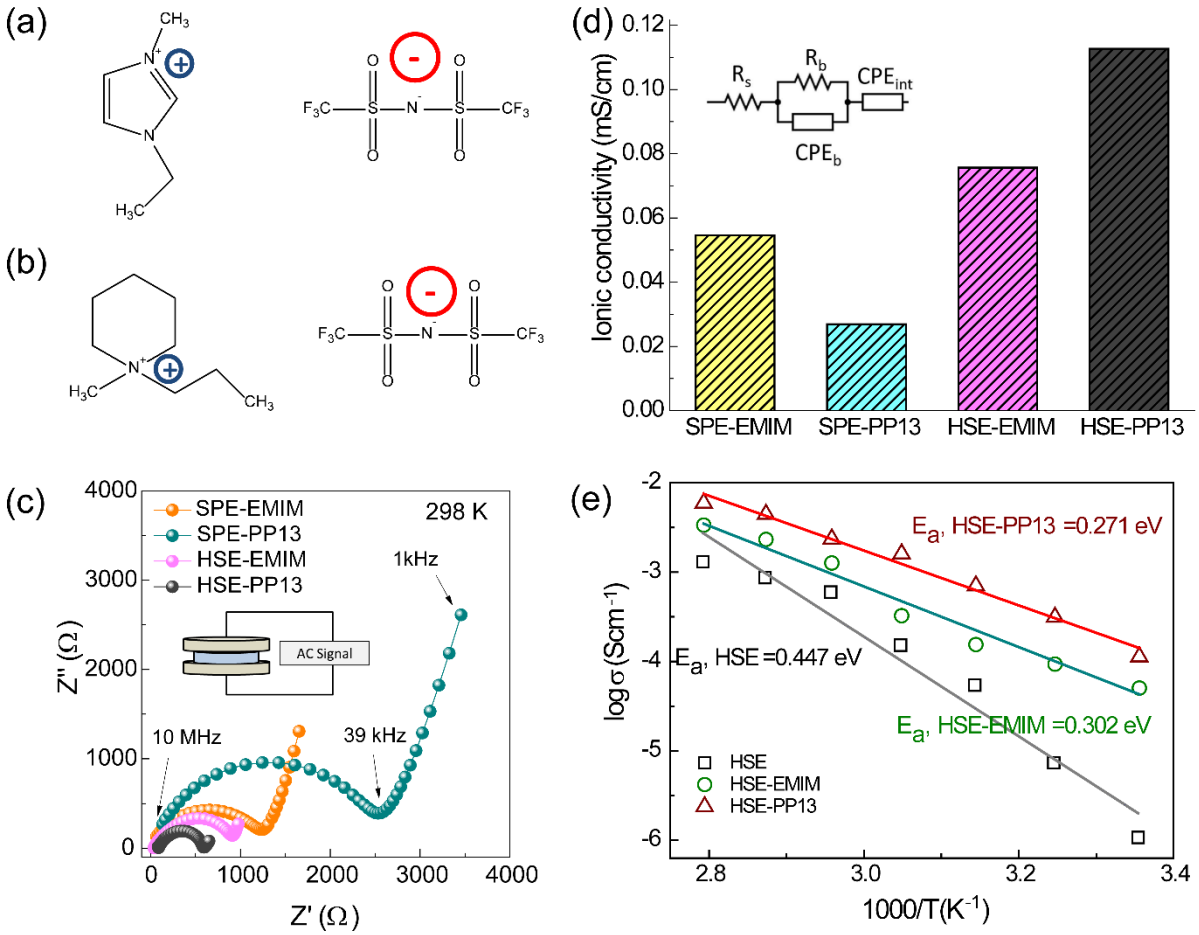

Figure 2 The macroscopic diffusion in HSE with PP13-TFSI and EMIM-TFSI ionic liquid additives. (a, b) Molecular structure of PP13-TFSI and EMIM-TFSI ionic liquids. **(c, d)** Electrochemical impedance spectroscopy measurements (EIS) and ionic conductivity of cells with LiTFSI-PEO solid polymer electrolytes with PP13-TFSI (SPE-PP13, 2.69×10^{-5} S/cm at 25 °C) and EMIM-TFSI (SPE-EMIM, 5.45×10^{-5} S/cm at 25 °C) ionic liquids, and LiTFSI-PEO-Li_6PS_5Cl HSEs with PP13-TFSI (HSE-PP13, 1.12×10^{-4} S/cm at 25 °C) and EMIM-TFSI (HSE-EMIM, 7.57×10^{-5} S/cm at 25 °C) ionic liquids. The contact area with the stainless steel current collector is 1.13 cm^2. (e) Ionic conductivity determined by impedance spectroscopy measurements of LiTFSI-PEO-Li_6PS_5Cl HSEs (E_a = 0.447 eV) and with PP13-TFSI (HSE-PP13, E_a = 0.271 eV) and EMIM-TFSI (HSE-EMIM, E_a = 0.302 eV) ionic liquids at varying temperatures.

To establish how the addition of the ILs improves the macroscopic conductivity of the PEO electrolyte (no Li_6PS_5Cl added) and of the HSEs, EIS measurements were performed. **Figure 2c** and **d** demonstrate that the conductivity of a mixture of a LiTFSI-PEO solid polymer electrolyte (SPE) with EMIM-TFSI (SPE-EMIM) is higher than that of the mixture with PP13-TFSI (SPE-PP13) as expected, due to the high miscibility of EMIM-TFSI with PEO, in good agreement with previous literature.[34] However, when Li_6PS_5Cl is introduced into the system, the opposite result is found. HSE-PP13 displays a higher conductivity compared to HSE-EMIM, also noting that both the HSEs have a higher conductivity than the materials without Li_6PS_5Cl. Also the activation energy indicates better conductivity for the HSE-PP13 electrolyte, where the variable temperature measurements shown in **Figure 2e** result in a lower activation energy, for HSE-PP13. Clearly, introduction of the inorganic Li_6PS_5Cl in the PEO matrix improved the overall conductivity, indicating that the Li_6PS_5Cl actively contributes to the conductivity.[10] Notably, the poorly miscible PP13-TFSI IL results in a higher conductivity of the HSE as compared to the more miscible EMIM-TFSI IL which improves the PEO conductivity.

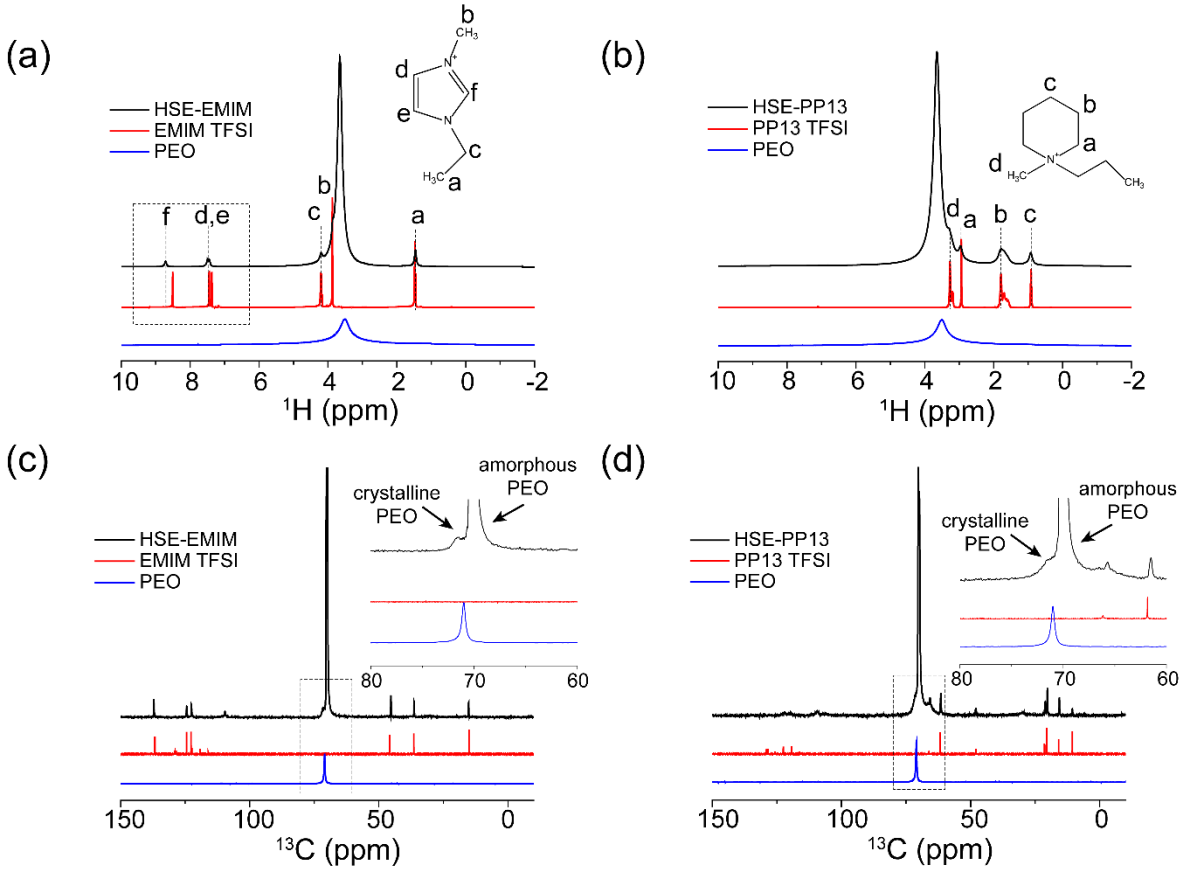

Figure 3 Structural characterization of the HSE with PP13-TFSI and EMIM-TFSI ionic liquids additives. (a, b) 1D ^{1}H spectra of LiTFSI-PEO-Li_6PS_5Cl HSE with EMIM-TFSI (HSE-EMIM) and PP13-TFSI (HSE-PP13) ionic liquids. ^{1}H spectra of PEO (solid), EMIM-TFSI (liquid), PP13-TFSI (liquid) are included for comparison. (c, d) ^{13}C Cross polarization (CP) MAS spectra of LiTFSI-PEO-Li_6PS_5Cl HSE with EMIM-TFSI (HSE-EMIM) and PP13-TFSI (HSE-PP13) ionic liquids. ^{13}C spectra of PEO (solid, CPMAS), EMIM-TFSI (liquid), PP13-TFSI (liquid) are included for comparison.

Impact of the ionic liquid on the bulk PEO and PEO-Li_6PS_5Cl interphase structure

To understand the improved conductivity of the HSE upon addition of the poorly miscible PP13-TFSI IL, the structure and kinetics of the PEO-Li_6PS_5Cl interface is investigated, which appears to play a critical role in activating the high conductivity of the Li_6PS_5Cl phase. The impact of adding the ILs to the bulk PEO structure is investigated first by comparing the ^{1}H and ^{13}C NMR spectra of the individual components. As shown in **Figure 3a**, the ^{1}H resonances of EMIM in HSE-EMIM for the peak positions between 6 to 10 ppm show a clear shift compared to pristine EMIM-TFSI, indicating a change in the ^{1}H environments on the imidazole ring.[36] No change is observed for PP13 (**Figure 3b**), reflecting the better miscibility of EMIM-TFSI in PEO.

Consistently, the chemical shift in the ^{13}C CPMAS spectra (**Figure 3c** and **d**), indicates less crystalline PEO in HSE-EMIM (70 ppm) compared to HSE-PP13 (72 ppm), consistent with the better miscibility of EMIM-TFSI in PEO,[37] further confirmed by the larger decrease in melting temperature when EMIM-TFSI is added (Supplementary **Text S1, Figure S4**)

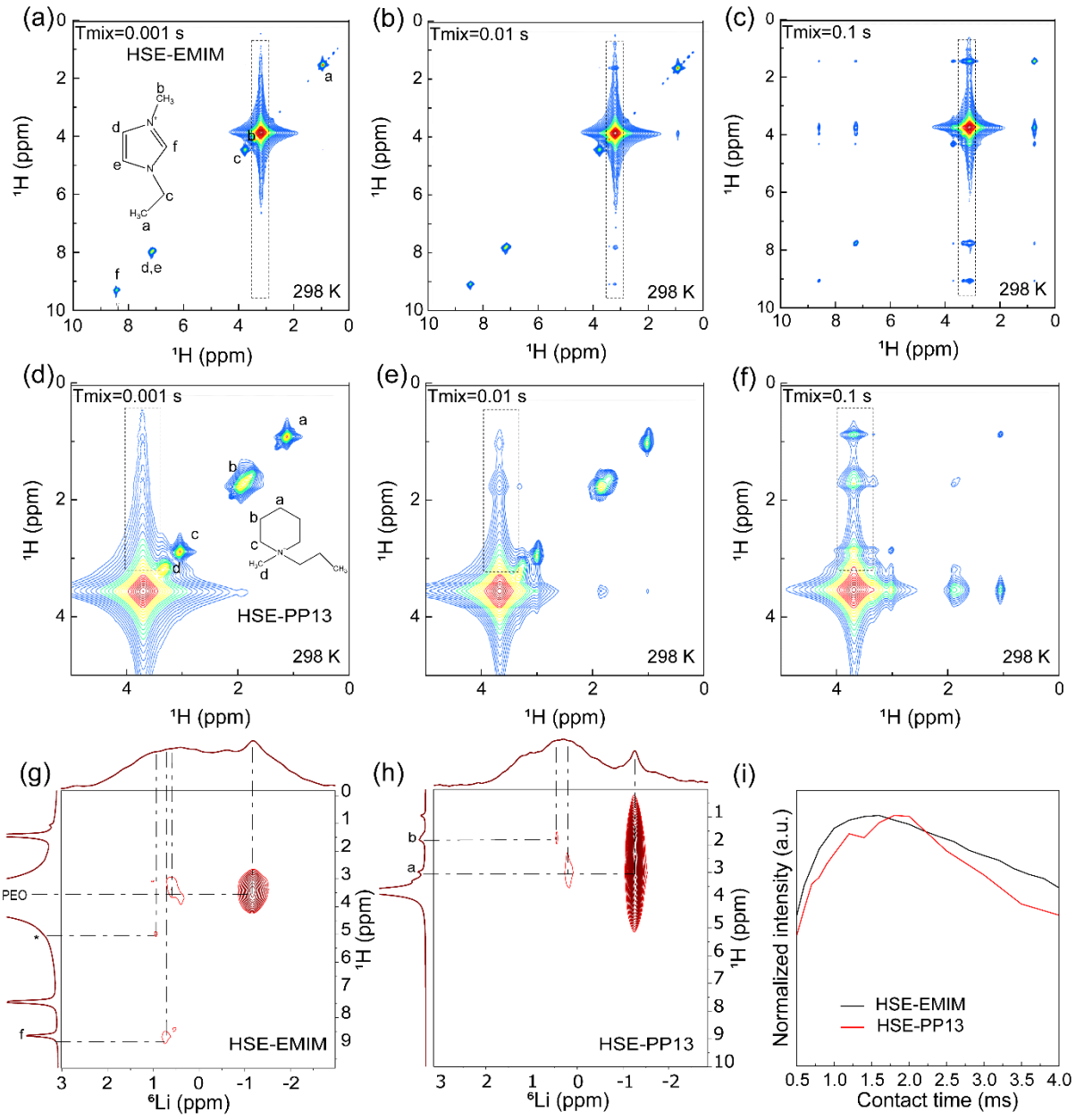

Figure 4 Locating the position of PP13-TFSI and EMIM-TFSI ionic liquids additives in the HSE. (a-f) 2D ^{1}H-^{1}H NOESY spectra of the mixture of LiTFSI-PEO-Li_6PS_5Cl with (a-c) EMIM-TFSI and (d-f) PP13-TFSI ionic liquid measured at a spinning speed of 5 kHz at 298 K with T_{mix} of 0.001, 0.01 and 0.1s. The dotted regions indicate the evolution of a series of cross peaks as a function of T_{mix}. (g, h) 2D ^{1}H-^{6}Li heteronuclear correlation (HETCOR) spectra of HSE-EMIM and HSE-PP13. (i) Integrated intensities taken from 1D ^{7}Li CPMAS spectra measured of the HSE-EMIM

and HSE-PP13 (representative spectra given in the supporting information **Figure S6**) at contact times from 200 µs to 4 ms of the Li-interface environment (located at ~0.26 ppm).

To understand the role of the IL in activating the LiTFSI-PEO-Li_6PS_5Cl interface, the interphase structure is explored using 2D ^1H-^1H nuclear overhauser effect spectroscopy (NOESY) NMR measurements, (**Figure 4a-f)**. NOESY is a commonly used method to elucidate polymer structures and configurations.[38] The cross peaks that arise, especially for short mixing times, are typically between protons that are in close spatial proximity (< 1 nm) to each other. As seen from **Figure 4a-c**, all the cross peaks between EMIM-TFSI and LiTFSI-PEO appear at nearly the same mixing time (Supplementary **Figure S5**)**,** indicating that there is no preferred orientation of the EMIM-TFSI species with respect to PEO, confirming the good miscibility and that the EMIM-TFSI is mobile. Interestingly for HSE-PP13 the ^1H-^1H correlations are first observed (short mixing times) between ^1H resonances at positions a and b on the piperidene ring of PP13-TFSI and the $–OCH_2$- protons from PEO (**Figure 4d-f**), which is especially clear from the intensity buildup shown in Supplementary **Figure S5**. These ring protons are the furthest away from the bulky propyl and methyl groups attached to the N atom on the piperidene ring. This indicates that the positively charged N atom on the piperidene ring, along with the functional groups it carries, are oriented away from the PEO segments.

Next, the interface environments in both HSEs are explored by 2D ^1H-^6Li HETCOR measurements (**Figure 4g** and **h**). This makes it possible to establish which Li-containing species are in proximity to the protons present in PEO and the ILs. For HSE-EMIM (**Figure 4g**) a strong correlation is found between PEO and LiTFSI, consistent with the solvation of EMIM in the PEO matrix. Additionally, PEO and EMIM (**Figure 2a**) correlate with the decomposed Li_6PS_5Cl surface species (observed for the HSE without IL, **Figure 1d**), indicating that a fraction of the PEO + EMIM is in contact with the Li_6PS_5Cl particles. For HSE-PP13 (**Figure 4h**), no correlations between PEO and LiTFSI or the decomposed Li_6PS_5Cl species are observed, the former consistent with poor solvation of this IL in PEO. However, correlations between the protons on the piperidene ring (**Figure 2b**) and LiTFSI as well as between the same protons of PP13 with the decomposed Li_6PS_5Cl surface environments are observed, indicating that PP13 is in contact with Li_6PS_5Cl. Finally, the PEO-Li_6PS_5Cl interface is further probed using ^1H–^7Li CPMAS experiments (**Figure 4i**), indicating that the PEO phase

is near the Li_6PS_5Cl interface for both HSE-PP13 and HSE-EMIM, but that there is a difference in proton kinetics between the two interfaces (see Supplementary **Text S2**, **Figure S6**, and **Table S1**).

To summarize, addition of EMIM-TFSI and PP13-TFSI result in a very different PEO bulk and interphase structure in the HSE. ^{1}H and ^{13}C NMR, as well as DSC measurements demonstrate that EMIM resides dominantly within the PEO, thereby lowering the PEO crystalline fraction. The ^{1}H-^{1}H NOESY spectra provide more detail, showing that EMIM has no preferred orientation towards PEO, whereas the PP13 does. 2D ^{1}H-^{6}Li HETCOR spectra demonstrate that PP13 is at the surface of the Li_6PS_5Cl, which in combination with the poor miscibility of PP13 in PEO established above, indicates that PP13 is predominantly located at the PEO-Li_6PS_5Cl interface, as initially hypothesized.

Impact of the ionic liquid on the interfacial diffusion between LiTFSI-PEO and Li_6PS_5Cl

To understand how the Li-ion diffusion (due to equilibrium charge transfer) over the PEO-Li_6PS_5Cl interface of the HSE is affected by both ILs, $^{6,7}Li$-$^{6,7}Li$ 2D EXSY NMR measurements are conducted, remembering that for the HSE without IL no Li-ion diffusion could be detected (**Figure 1b-c**). For HSE-EMIM (Supplementary **Figure S7a** and **b**), no cross peaks are observed with mixing times as long as 2 s, indicating that there is no significant Li-ion diffusion over the LiTFSI-PEO-Li_6PS_5Cl interface at this timescale. In contrast, clear cross peaks, corresponding to Li-ion diffusion between the LiTFSI-PEO and Li_6PS_5Cl phases, appear for HSE-PP13 (**Figure 5** and Supplementary **Figure S7c** and **d**). This indicates more facile diffusion over the organic-inorganic interface in the HSE-PP13, which is associated with the presence of the PP13 at the PEO-Li_6PS_5Cl interface established in the previous section.

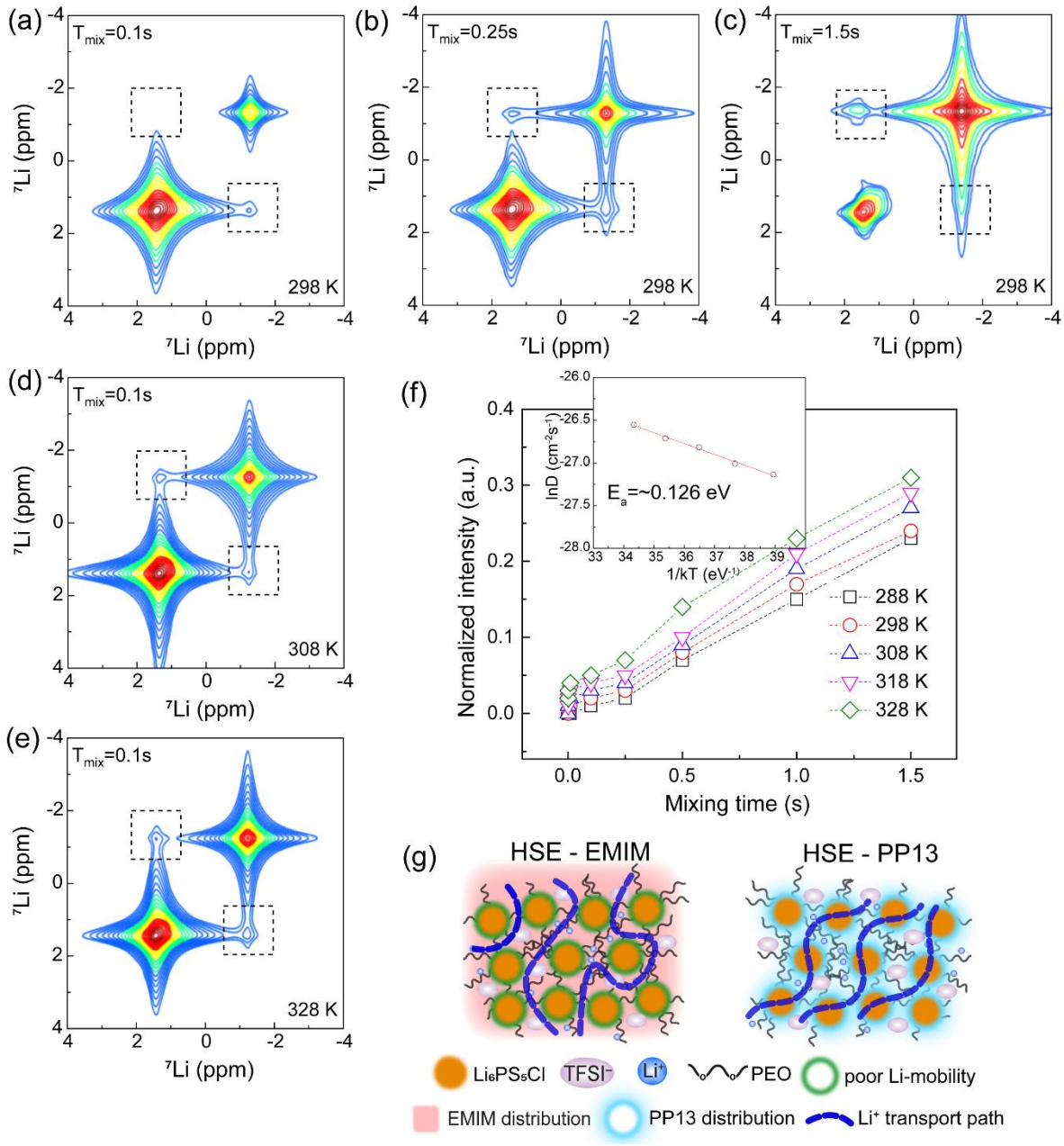

Figure 5 Quantification of Li-ion diffusion across phase boundaries in the HSE with the PP13-TFSI ionic liquid. (a-e) 2D ^{7}Li-^{7}Li EXSY spectra of the mixture of LiTFSI-PEO-Li_6PS_5Cl with PP13-TFSI ionic liquid measured at spinning speed of 5 kHz at (a-c) 298 K with mixing times T_{mix} of 0.1, 0.25 and 1.5 s, and (d, e) at 308 and 328 K with a T_{mix} of 0.1 s. (f) Evolution of cross peak intensity as a function of T_{mix} obtained from the 2D-EXSY measurements done at the temperatures indicated in the graph. The line passing through the symbols is a guide to the eye. Inset figure is the dependence of the diffusion coefficient (D) obtained from fitting the data in (f) to a diffusion model described by us in detail elsewhere.[30] These can be fit with the Arrhenius law, yielding an activation energy (E_a) of 0.126 eV. (g) Proposed Mechanism for Li-ion diffusion in HSE with EMIM-TFSI and PP13-TFSI ionic liquids additives.

Upon increasing the mixing time and the temperature a clear increase in cross-peak intensity is observed (**Figures 5a-e**). The Li-ion exchange between the LiTFSI-PEO and Li_6PS_5Cl phases was quantified by fitting the evolution of the cross peak intensity as a function of T_{mix} (see Supplementary **Text S3**, **Figure 5f**) to a diffusion model derived from Fick's law, described elsewere.[29,30,39] The diffusion coefficient as a function of temperature obtained from the fit (inset **Figure 5f**), reflects the Li-ion self-diffusion across the LiTFSI-PEO-Li_6PS_5Cl interface. Fitting with an Arrhenius law, yields an activation energy of 0.126 eV for diffusion between the organic and inorganic components, significantly lower than that reported with impedance.[26,27] This suggests that addition of the PP13-TFSI IL 'activates' the LiTFSI-PEO-Li_6PS_5Cl interface, even though micron-sized inorganic argyrodite filler particles are used in the HSE, thus having a relatively small ionic contact area.

Based on these observations we can now link the PEO-Li_6PS_5Cl interface nanostructure, with the Li-ion mobility over the interface. The poor diffusivity over the interface between PEO and Li_6PS_5Cl in the HSE can be rationalized by the observed $–OCH_2–$ groups at the interface, (**Figure 1**), which annihilates the conducting ethereal oxygen positions that mediate the Li-ion conductivity in PEO. The consequence is that Li-ion transport will be forced though the polymer phase, not utilizing the high conductivity of the Li_6PS_5Cl phase (**Figure 5g**). In contrast to the miscible EMIM-TFSI which improves the conductivity of the PEO, the much less miscible PP13-TFSI settles at the interface with the Li_6PS_5Cl phase (**Figure 5g**), where it leads to a higher local mobility. This is held responsible for the facile Li-ion diffusivity over the PEO-Li_6PS_5Cl interface as quantified by the 2D EXSY experiments in **Figure 5.** This can be explained by the higher local mobility induced by the PP13 IL but also the higher dielectric constant of the IL ($\epsilon > 20$) compared to PEO ($\epsilon \sim 5$) may play a role,[40] thus enhancing the local polarizability. Facilitated by the higher Li-ion diffusivity over the inorganic-organic interface in the presence of PP13-TFSI, long range Li-ion transport can now make use of the much higher conductivity of the Li_6PS_5Cl phase (**Figure 5g**), which explains the higher overall conductivity of the HSE-PP13 electrolyte observed with EIS (**Figure 2c-d**).

Electrochemical evaluation of the hybrid solid electrolyte upon introduction of ionic liquids

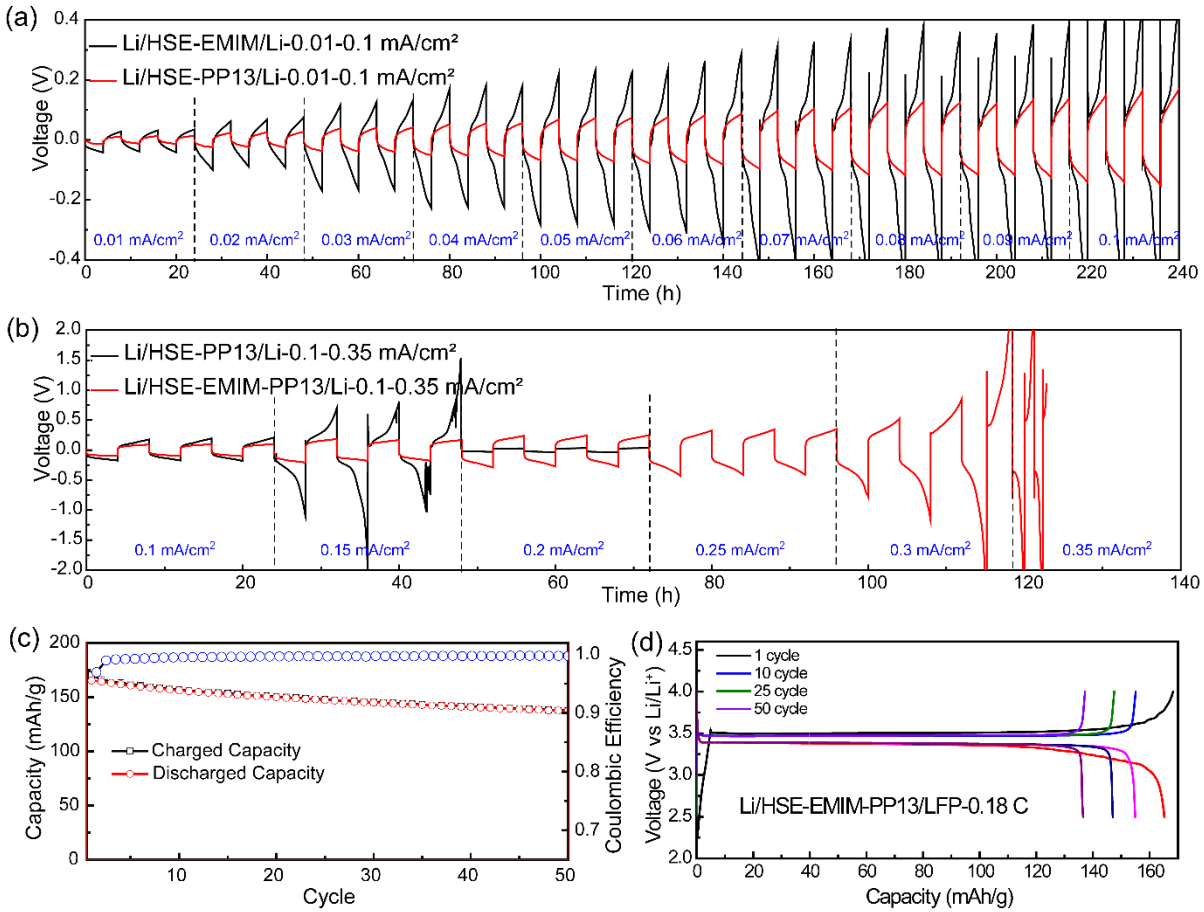

Figure 6 Electrochemical characterization of the HSE with PP13-TFSI and EMIM-TFSI ionic liquid additives (a) Plating and stripping curves of a Li metal symmetrical cell (Li/HSE/Li) with LiTFSI-PEO-Li_6PS_5Cl HSEs only with PP13-TFSI (HSE-PP13) or EMIM-TFSI (HSE-EMIM) ionic liquids measured at room temperature. (b) Plating and stripping curves of symmetrical cell with LiTFSI-PEO-Li_6PS_5Cl HSE only with PP13-TFSI and a mixture of PP13-TFSI and EMIM-TFSI (PP13-TFSI and EMIM-TFSI, 0.25:1 molar ratio IL:Li-ion, HSE-PP13-EMIM) ionic liquids measured at room temperature. (c) Specific charge/discharge capacity and Coulombic efficiency as a function of cycle number and (d) charge and discharge voltage curves of a $LiFePO_4$/HSE-EMIM-PP13/Li battery cycled at 0.18 C and at room temperature.

Because Li-metal is the ultimate anode from the perspective of battery energy density, the impact of the IL on the interface of the HSE with Li metal is evaluated in Li-metal symmetrical cells for both HSE-PP13 and HSE-EMIM electrolytes (**Figure 6**). The over-potential of the symmetrical cell is an indicative parameter of the interface stability and ability to conduct Li-ions.[25] In **Figure 6a**, the Li/HSE-EMIM/Li cell shows a continuous increase in over-potential when the current density is higher than 0.05 mA/cm^2, indicating insufficient Li-ion conductivity. In contrast the Li/HSE-PP13/Li cell

shows a much more stable over-potential, increasing with current density up to a relatively small value, not exceeding 200 mV at 0.1 mA/cm^2. A similar trend is observed upon cycling (Supplementary **Figure S8**). Taking it one step further, we can assume that in the HSE-PP13 electrolyte, the conductivity is no longer limited by the PEO-Li_6PS_5Cl interface due to the presence of PP13, but by the polymer phase. To evaluate this, an HSE is prepared with both the PP13-TFSI and EMIM-TFSI additives. In this HSE, PP13 will enhance the interfacial Li-ion diffusivity while EMIM is expected to enhance the Li-ion diffusivity in the PEO phase by improving the chain mobility. Indeed, the small fraction of IL mixture increases the ionic conductivity to 2.47×10^{-4} S/cm at 25 °C as measured by EIS (Supplementary **Figure S9**). The higher conductivity upon adding both ILs is accompanied by a higher critical current density of 0.25 mA/cm^2 (**Figure 6b**) as compared to addition of the individual IL additives (**Figure 6a**). In theory, a critical current density of 0.25 mA/cm^2 could already enable a solid-state battery using Li-S as cathode having an energy density more than 500 Wh/kg.[41] The HSE with both ILs added demonstrates a critical current density compared to state-of-the-art solid-state electrolytes reported in literature (Supplementary **Table S2**), although realizing that this is achieved by a small fraction of a liquid (IL) phase. Finally, the HSE with the dual IL additives was electrochemically cycled in a Li metal battery in combination with a $LiFePO_4$ cathode (**Figure 6c** and **d**). The battery delivers a capacity of more than 0.8 mAh (120 mAh/g) after 50 cycles, with an average Coulombic efficiency of ~ 99.9 % and an overpotential of 150 mV, indicating the feasibility of this HSE to function as a solid-state electrolyte for a room temperature Li metal battery.

Conclusions

In conclusion, we propose that the bottleneck for Li-ion transport in HSEs comprising of PEO polymer and inorganic solid electrolyte phases is across the organic-inorganic phase boundaries, where the deficiency of ethereal oxygen species and absence of local mobility are held responsible for the poor local Li-ion conductivity at the interface. The interface diffusivity can be improved by making use of an IL additive as a wetting agent, in this case PP13-TFSI, whose low miscibility in PEO forces it to be positioned at the phase boundaries where it functions as a bridge for Li-ion transport. The multinuclear solid-state NMR investigation reveals the structure of the interface between the organic and inorganic phases in the HSE and how this affects the Li-ion diffusion pathway. This sheds light on the development of interface strategies, such as

the one proposed with non-miscible ILs, leading to improved conductivities and compatibility with Li-metal anodes.

Acknowledgements

The authors thank Frans Ooms, Fengqi Zhang and Chao Ma for their assistance with experiments. M.L. and M.W. acknowledge the financial support from the Netherlands Organization for Scientific Research (NWO) under the VICI grant nr. 16122. E.v.E. further acknowledge NWO for their support of the solid-state NMR facility for advanced materials science, which is part of the uNMR-NL grid (NWO grant 184.035.002). M.W. gratefully acknowledge the financial support from the Advanced Dutch Energy Materials (ADEM) program of the Dutch Ministry of Economic Affairs, Agriculture and Innovation.

Author Contributions

S.G. and M.W. designed and supervised the research. M.L., S.Z. and C.W. synthesized and characterized the hybrid solid electrolytes. M.L. and S.Z. carried out the electrochemical measurements. M.L., S.G. and E.v.E. measured and analysed the NMR data. M.L., S.G. and M.W. wrote the manuscript.

Competing Interests

The authors declare no competing interests.

References

1 Armand, M. & Tarascon, J.-M. Building better batteries. *Nature* **451**, 652-657 (2008).

2 Dunn, B., Kamath, H. & Tarascon, J.-M. Electrical energy storage for the grid: a battery of choices. *Science* **334**, 928-935 (2011).

3 Cheng, X. B., Zhao, C. Z., Yao, Y. X., Liu, H. & Zhang, Q. Recent Advances in Energy Chemistry between Solid-State Electrolyte and Safe Lithium-Metal Anodes. *Chem* **5**, 74-96 (2019).

4 Zaman, W., Hortance, N., Dixit, M. B., De Andrade, V. & Hatzell, K. B. Visualizing percolation and ion transport in hybrid solid electrolytes for Li-metal batteries. *J Mater Chem A* **7**, 23914-23921 (2019).

5 Armand, M. The history of polymer electrolytes. Solid State Ionics **69**, 309-319 (1994).

6 Bouchet, R. *et al.* Single-ion BAB triblock copolymers as highly efficient electrolytes for lithium-metal batteries. *Nature Materials* **12**, 452-457 (2013).

7 Ma, Q. *et al.* Single lithium-ion conducting polymer electrolytes based on a super-delocalized polyanion. *Angewandte Chemie International Edition* **55**, 2521-2525 (2016).
8 Dixit, M. B. *et al.* Scalable Manufacturing of Hybrid Solid Electrolytes with Interface Control. *Acs Appl Mater Inter* **11**, 45087-45097(2019).
9 Osada, I., de Vries, H., Scrosati, B. & Passerini, S. Ionic-liquid-based polymer electrolytes for battery applications. *Angewandte Chemie International Edition* **55**, 500-513 (2016).
10 Liu, M. *et al.* Tandem Interface and Bulk Li-Ion Transport in a Hybrid Solid Electrolyte with Microsized Active Filler. *ACS Energy Lett* **4**, 2336-2342 (2019).
11 Yang, K. *et al.* Stable Interface Chemistry and Multiple Ion Transport of Composite Electrolyte Contribute to Ultra-long Cycling Solid-State $LiNi_{0.8}Co_{0.1}Mn_{0.1}O_2$/Lithium Metal Batteries. *Angewandte Chemie International Edition* **60**, 24668-24675, (2021).
12 Croce, F., Sacchetti, S. & Scrosati, B. Advanced lithium batteries based on high-performance composite polymer electrolytes. *J Power Sources* **162**, 685-689 (2006).
13 Syzdek, J. *et al.* Ceramic-in-polymer versus polymer-in-ceramic polymeric electrolytes-A novel approach. *J Power Sources* **194**, 66-72 (2009).
14 Hassoun, J. & Scrosati, B. A high-performance polymer tin sulfur lithium ion battery. *Angewandte Chemie International Edition* **49**, 2371-2374 (2010).
15 Płcharski, J. & Weiczorek, W. PEO based composite solid electrolyte containing nasicon. *Solid State Ionics* **28**, 979-982 (1988).
16 Xu, K. Electrolytes and interphases in Li-ion batteries and beyond. *Chemical Review* **114**, 11503-11618 (2014).
17 Lei, D. *et al.* Cross-linked beta alumina nanowires with compact gel polymer electrolyte coating for ultra-stable sodium metal battery. *Nature Communications* **10**, 4244 (2019).
18 Zheng, J., Tang, M. X. & Hu, Y. Y. Lithium Ion Pathway within $Li_7La_3Zr_2O_{12}$-Polyethylene Oxide Composite Electrolytes. *Angewandte Chemie International Edition* **55**, 12538-12542, (2016).
19 Wang, S. *et al.* A dendrite-suppressed flexible polymer-in-ceramic electrolyte membrane for advanced lithium batteries. *Electrochim Acta* **353** (2020).
20 Fergus, J. W. Ceramic and polymeric solid electrolytes for lithium-ion batteries. *J Power Sources* **195**, 4554-4569 (2010).
21 Blanga, R., Burstein, L., Berman, M., Greenbaum, S. & Golodnitsky, D. Solid polymer-in-ceramic electrolyte formed by electrophoretic deposition. *Journal of The Electrochemical Society* **162**, D3084-D3089 (2015).
22 Chen, L. *et al.* PEO/garnet composite electrolytes for solid-state lithium batteries: From "ceramic-in-polymer" to "polymer-in-ceramic". *Nano Energy* **46**, 176-184 (2018).
23 Huo, H. Y. *et al.* Rational Design of Hierarchical "Ceramic-in-Polymer" and "Polymer-in-Ceramic" Electrolytes for Dendrite-Free Solid-State Batteries. *Adv Energy Mater* **9,** 1804004 (2019).
24 Bonizzoni, S. *et al.* NASICON-type polymer-in-ceramic composite electrolytes for lithium batteries. *Physical Chemistry Chemical Physics* **21**, 6142-6149 (2019).
25 Dixit, M. B. *et al.* Nanoscale Mapping of Extrinsic Interfaces in Hybrid Solid Electrolytes. *Joule* **4**, 207-221(2020).

26 Simon, F. J. *et al.* Properties of the interphase formed between argyrodite-type Li_6PS_5Cl and polymer-based PEO_{10}: LiTFSI. *ACS applied materials & interfaces* **11**, 42186-42196 (2019).
27 Simon, F. J., Hanauer, M., Richter, F. H., Janek, J. r. J. A. A. M. & Interfaces. Interphase Formation of PEO_{20}: LiTFSI–Li_6PS_5Cl Composite Electrolytes with Lithium Metal. *ACS applied materials & interfaces* **12**, 11713-11723 (2020).
28 Zheng, J., Wang, P., Liu, H. & Hu, Y.-Y. Interface-enabled ion conduction in $Li_{10}GeP_2S_{12}$–poly (ethylene oxide) hybrid electrolytes. *ACS Applied Energy Materials* **2**, 1452-1459 (2019).
29 Yu, C. *et al.* Accessing the bottleneck in all-solid state batteries, lithium-ion transport over the solid-electrolyte-electrode interface. *Nat Commun* **8**, 1086, doi:10.1038/s41467-017-01187-y (2017).
30 Ganapathy, S., Yu, C., van Eck, E. R. H. & Wagemaker, M. Peeking across Grain Boundaries in a Solid-State Ionic Conductor. *ACS Energy Lett* **4**, 1092-1097 (2019).
31 Schwietert, T. K. *et al.* Clarifying the relationship between redox activity and electrochemical stability in solid electrolytes. *Nature Materials* **19**, 428-435, (2020).
32 Hoefling, A. *et al.* Mechanism for the Stable Performance of Sulfur-Copolymer Cathode in Lithium–Sulfur Battery Studied by Solid-State NMR Spectroscopy. *Chemistry of Materials* **30**, 2915-2923, (2018).
33 Rataboul, F. *et al.* Molecular Understanding of the Formation of Surface Zirconium Hydrides upon Thermal Treatment under Hydrogen of [(≡ SiO) Zr (CH_2 t Bu) $_3$] by Using Advanced Solid-State NMR Techniques. *Journal of the American Chemical Society* **126**, 12541-12550 (2004).
34 Zhu, C., Cheng, H. & Yang, Y. Electrochemical characterization of two types of PEO-based polymer electrolytes with room-temperature ionic liquids. *Journal of the Electrochemical Society* **155**, A569 (2008).
35 Kodama, K. *et al.* Structural effects of polyethers and ionic liquids in their binary mixtures on lower critical solution temperature liquid-liquid phase separation. *Polymer journal* **43**, 242-248 (2011).
36 Cesare Marincola, F. *et al.* NMR Investigation of Imidazolium-Based Ionic Liquids and Their Aqueous Mixtures. *ChemPhysChem* **13**, 1339-1346 (2012).
37 Wang, B.-H., Xia, T., Chen, Q. & Yao, Y.-F. Probing the Dynamics of Li^+ Ions on the Crystal Surface: A Solid-State NMR Study. *Polymers* **12**, 391 (2020).
38 Zhao, Z. *et al.* Ionic-Association-Assisted Viscoelastic Nylon Electrolytes Enable Synchronously Coupled Interface for Solid Batteries. *Advanced Functional Materials* **30**, 2000347 (2020).
39 Ganapathy, S., van Eck, E. R., Kentgens, A. P., Mulder, F. M. & Wagemaker, M. Equilibrium Lithium-Ion Transport Between Nanocrystalline Lithium-Inserted Anatase TiO2 and the Electrolyte. *Chemistry–A European Journal* **17**, 14811-14816 (2011).
40 Kumar, M. & Sekhon, S. J. E. P. J. Role of plasticizer's dielectric constant on conductivity modification of PEO–NH_4F polymer electrolytes. *European Polymer Journal* **38**, 1297-1304 (2002).
41 Liu, M. *et al.* Novel gel polymer electrolyte for high-performance lithium-sulfur batteries. *Nano Energy* **22**, 278-289 (2016).
42 Fung, B., Khitrin, A. & Ermolaev, K. An improved broadband decoupling sequence for liquid crystals and solids. *Journal of magnetic resonance* **142**, 97-101 (2000).

Methods

The solid-state electrolyte Li_6PS_5Cl was prepared by a simple solid-state reaction. The stoichiometric raw materials LiCl (Sigma-Aldrich), P_2S_5 (Sigma-Aldrich), and Li_2S (Sigma-Aldrich) were used as the starting materials and were ball milled at 110 rpm, 2hrs with the ZrO_2 coated jars using 18 ZrO_2 balls. After the ball milling, the precursor was sealed in a quartz tube with Ar and then annealed at 550 ^oC for 15 hours to obtain the Li_6PS_5Cl solid electrolyte.

Hybrid solid electrolyte (HSE) films were prepared by mixing 0.768 g PEO (Sigma-Aldrich, M_w=600,000), 0.28 g LiTFSI (Sigma-Aldrich), 0.1048 g Li_6PS_5Cl and 0.25:1 molar ratio IL:Li-ion of ionic liquid together in 10 ml acetonitrile (Sigma-Aldrich) and stirring for 24 h. The prepared solution was evenly casted on a Teflon plate and dried in the glove box at room-temperature for 24 h, then transfer into vacuum environment in glove box for 48 h. Differential scanning calorimetry (DSC) measurements were carried out at 10 degree/min steps using a commercial TA-Q2000 DSC calorimeter. The morphology of HSE was analyzed by Scanning Electron Microscope (SEM, JEOL JSM IT100LA).

LSV was performed to cell of Li/HSE/SS with stainless steel (SS) area of 1.13 cm^2. The LSV curves were recorded from OCV to 5.5 V versus Li/Li-ion at a scanning rate of 0.1 mV s^{-1} using an Autolab (PGSTAT302N). The ionic conductivities of the HSEs were measured by EIS where the HSE is sandwiched between two stainless steel blocking electrodes (area of 1.13 cm^2), kept at each test temperature (from 25 to 85 °C) for at least half an hour before the electrochemical impedance measurements were acquired, in order to reach thermal equilibrium. The EIS measurements were carried out by an Autolab (PGSTAT302N) in the frequency range of 10 MHz–1 kHz with a sinusoidal signal with V_{rms} = 10 mV. EIS spectra were fit with an equivalent circuit (EC) model, where R_S is the series resistance, R_b is the bulk polymer resistance, CPE_b is a constant phase element (CPE) which accounts for the bulk capacitance of the polymer film, and CPE_{int} accounts for the capacitance associated with the blocking electrodes at low frequencies. From that the bulk resistance (R_b) and the ionic conductivity (σ) is calculated by using the equation: $\sigma = d / (R_b \times A)$; where d is the thickness, and A is the area of polymer electrolyte contacting with the stainless steel (1.13 cm^2 in our case). The HSE-based all-solid-state cells were assembled in an Ar-

filled glove box. These cells consisted of of lithium metal (Aldrich) and $LiFePO_4$ (mass loading: ~6.5 mg/cm^2) as electrodes, and the HSE as the electrolyte. It should be noted that 50 µL of the HSE solution prepared with above methods was dropped into an LFP electrode and then fully allowed to dry. $LiFePO_4$ (Sigma-Aldrich) cathodes were prepared by mixing the active material with Super P and PVDF in a mass ratio of 8:1:1, and NMP was used as a solvent. Charge-discharge tests of the HSE-based all-solid-state cells were carried out using a Maccor 4000 battery cycler at room temperature.

Solid-state NMR measurements were performed on a Bruker Ascend 500 magnet (B_0 = 11.7 T) with a NEO console operating at frequencies of 500.130 MHz for ^{1}H, 194.37 MHz for ^{7}Li, 73.6 MHz for ^{6}Li and 125.758 for ^{13}C. ^{6,7}Li chemical shifts were referenced with respect a 0.1 M LiCl solution (0 ppm) and ^{1}H and ^{13}C chemical shifts were referenced with respect to solid adamantane (^{1}H at 1.81 ppm and ^{13}C at 38.48 ppm). A Bruker three channel MAS 4 mm DVT probe was used for all measurements. The LiTFSI-PEO-Li_6PS_5Cl (HSE), HSE-EMIM, and HSE-PP13 membranes were cut into tiny pieces and filled in 4 mm zirconia rotors, which were spun at spinning speeds of 5 kHz for all measurements. One pulse ^{1}H, ^{7}Li and ^{6}Li experiments were performed with $\pi/2$ pulse lengths of 3.5, 2.7, and 4.75 µs respectively. A recycle delay of three times of T_1 was used each time, where T_1 was determined using saturation recovery experiments. Two-dimensional (2D) ^{7}Li-^{7}Li and ^{6}Li-^{6}Li exchange spectroscopy (EXSY) measurements were performed for these samples at various mixing times from 1 ms up to 2 s and at temperatures from 10 to 50 ^{0}C. Each spectrum consisted of 8(16) scans for each of the 1200-1500 (400-800) transients, each transient incremented by 200(400) µs with a recycle delay of up to 5(10) s. The ^{6}Li CPMAS experiments were performed with an initial ^{1}H $\pi/2$ pulse of 5 µs. During cross polarization, for ^{6}Li, rf field strengths of 25 kHz and contact times of up to 6 ms were utilized. The rf field amplitude of ^{1}H during CP was ramped from 70 to 100%. 256(1024) scans were acquired for each sample with a recycle delay of 2(3) s. 2D ^{1}H-^{6}Li heteronuclear correlation (HETCOR) measurements were performed with a short CP contact time of 0.2 ms for the HSE and long contact times of 10 ms each for the HSE-EMIM and HSE-PP13. For each of the 128 transients in the indirect ^{1}H dimension, 128 ^{6}Li scans were accumulated. A recycle delay of 3 s was applied after each scan. The ^{13}C CPMAS experiments were measured with an initial ^{1}H $\pi/2$ pulse of 3.65 µs. During cross polarization for ^{13}C, an rf field strengths of 58 kHz was utilized. 40000 scans were

acquired for each sample with a recycle delay of 2 s. For both the CPMAS and HETCOR experiments, proton decoupling was performed during acquisition using the SPINAL-64 decoupling sequence.[42] 2D ^{1}H-^{1}H NOESY measurements were performed at various mixing times from 1 ms to 100 ms at room temperature. Each spectrum consisted of 8 scans for each of the 800 transients, each transient incremented by 100 μs with a recycle delay of 2 s. ^{7}Li CPMAS experiments were performed on an Agilent 400 MHz spectrometer operating at 155.422 MHz for ^{7}Li and 399.915 MHz for ^{1}H. A 4mm HXY chemagnetics pencil design probe was used at an MAS speed of 5 kHz. For cross polarization both the ^{1}H and ^{7}Li RF-field strength was set at 40 kHz and Spinal-64 proton decoupling at the same field strength with 12.5 μs pulselength and a 8^{o} phase shift was used during acquisition.

Data availability

The data that support the findings of this study are available at the online depository Zenodo (https;//doi.org/10.5281/zenodo.6334099)